WPEDU-PR(18) 21325

F. Manke et al.

Time intermittency in non-diffusive transport regimes of fast ions in turbulent plasmas

Preprint of Paper to be submitted for publication in
Physical Review E

This work has been carried out within the framework of the EUROfusion Consortium and has received funding from the Euratom research and training programme 2014-2018 under grant agreement No 633053. The views and opinions expressed herein do not necessarily reflect those of the European Commission.

Time intermittency in non-diffusive transport regimes of fast ions in turbulent plasmas

F. Manke,[1,*] M. Baquero-Ruiz,[1] I. Furno,[1] O. Chellaï,[1] A. Fasoli,[1] and P. Ricci[1]

[1] *École Polytechnique Fédérale de Lausanne (EPFL), Swiss Plasma Center (SPC), CH-1015 Lausanne, Switzerland*

(Dated: January 24, 2019)

Intermittent phenomena have long been studied in the context of non-diffusive transport across a variety of fields. In the TORPEX device, the cross-field spreading of an injected fast ion beam by electrostatic plasma turbulence can access different non-diffusive transport regimes. A comprehensive set of fast ion time-series has been acquired and time intermittency quantified by their skewness. Values distinctly above background level are found across all observed transport regimes. Intermittency tends to increase toward quasi- and superdiffusion and for longer fast ion propagation times. The motion of a concentrated instantaneous beam within a larger mean profile determines the specific prevalence of intermittency. We demonstrate the effectiveness of an analytical model developed to predict local intermittency from the mean profile.

I. INTRODUCTION

The motion of single or a collection of particles (such as fluid elements) is often termed *intermittent* in time when it features extended waiting-times between brief, irregular occurrences of strong activity. Particularly in turbulence, the formation of distinct coherent structures has long been characterized as intermittent [1, 2]. When averaging across a given particle distribution, intermittent behavior and the associated non-gaussian statistics of motion can result in a non-linear scaling of the particle mean square displacement with time, $\langle \Delta x^2 \rangle \sim t^\nu$, with $\nu \neq 1$ [3]. In models for this *non-diffusive* transport, the heavy-tailed waiting time distributions often lead toward subdiffusion ($\nu < 1$)[3–5]. Intermittency in subdiffusive transport has been studied in a variety of fields, from space-physics [6], to material aging [7] or sediment transport [8]. Superdiffusion ($\nu > 1$) can only arise from a competition with heavy-tailed jump length distributions [3]. Intermittency in superdiffusive transport has been reported e.g. in conjunction with the formation of coherent structures in atmospheric [9], or plasma turbulence [10–12]. In purely mathematical studies, it has been demonstrated that any regime of non-diffusive transport can be generated through intermittency in simple functional mappings [13–15]. Likewise, certain biological systems can exhibit either super- or subdiffusive behavior as a result of intermittent motion [16]. However, the general question of whether super- or subdiffusion can be inferred from local observations of intermittency is still open.

In this paper, we investigate time intermittency of fast ions injected into turbulent plasmas in the TORoidal Plasma Experiment (TORPEX, see Fig. 1) [17–19]. The spreading of the fast ion beam exhibits a smooth transition between super-, quasi- and subdiffusive transport regimes [20, 21]. Using first three-dimensional measurements of the local fast ion time-series, we systematically quantify the prevalence of time intermittency by measuring the time-series' skewness across all the observed non-diffusive transport regimes. We introduce an analytical model [22] for the fast ion beam motion, which allows us to predict the skewness of these time-series based solely on their mean value across various transport regimes.

The paper is organized as follows: Sec. II introduces the TORPEX device in detail, with a focus on the fast ion experiments. In Sec. III, we present the principal experimental measurements of the fast ion beam and time intermittency across different non-diffusive transport regimes. Sec. IV adapts the analytical model we developed in [22] and demonstrates its predictive effectiveness by fitting predicted time-series statistics to the measurements. Finally we summarize our findings in Sec. V.

II. EXPERIMENTAL METHODS

A. The TORPEX device

TORPEX is a basic plasma physics device, with major radius $R_0 = 1\,\mathrm{m}$ and minor radius $a = 0.2\,\mathrm{m}$, featuring helical open magnetic field-lines. Our experimental setup and coordinate convention is shown in Fig. 1.

The toroidal field on-axis is $B_\Phi = 74\,\mathrm{mT}$ and the vertical field $B_v \approx 2\,\mathrm{mT}$, leading to a magnetic pitch angle of $\lesssim 2°$. A hydrogen plasma with temperatures of $T_e \approx 2.5\,\mathrm{eV}$ and $T_i < 1\,\mathrm{eV}$ (for electrons and ions respectively) and densities $n_e = n_i \approx 10^{16}\,\mathrm{m}^{-3}$ is generated through microwave injection at 2.45 GHz, which lies in the electron-cyclotron (EC) range [24]. With the EC resonance layer on the High-Field-Side (HFS) typically at $R \approx -12\,\mathrm{cm}$ and a nearby Upper Hybrid resonance, strong density fluctuations from an interchange-mode are present near $R \approx -10\,\mathrm{cm}$ due to the radial density and temperature gradients [25–27]. This mode is the source of strong electrostatic plasma turbulence towards the center of the device. Intermittently, coherent field-aligned structures (so-called 'blobs') [17, 28, 29] are generated. These blobs propagate towards the Low-Field-Side (LFS) due to their dipole-like nature and the associated $\mathbf{E}\times\mathbf{B}$-

* fabian.manke@epfl.ch

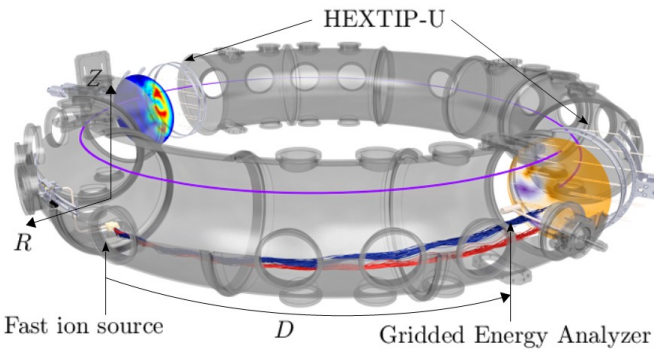

FIG. 1. Fast ion experimental set-up in TORPEX. The poloidal coordinates R and Z are indicated, with $R = Z = 0$ on axis and the toroidal source-detector distance D. The Gridded Energy Analyzer (GEA) can be displaced over most of the poloidal cross-section. Fast ion trajectories are shown in red for an injection energy E of 30 eV, in dark blue for 70 eV. A magnetic field-line is indicated in purple. A plasma density profile interpolated from ion-saturation current measurements with the Langmuir probe arrays HEXTIP-U [23] is shown on the left, its floating potential profile on the right.

drift [28–30]. This well characterized plasma scenario is the starting point for the study of non-diffusive fast ion transport.

B. Fast ion studies

Fast ions are injected toroidally by thermal emission from a lithium-6 ion source delivering $\approx 10\,\mu$A of ion-current under bias. The bias of the source itself as well as 2 successive grids is set to maintain the injected current while accelerating the ions in the toroidal direction to energies E of typically either 30 eV or 70 eV, and thus produce a fast ion beam. The ion source is mounted at $R = -1$ cm and $Z = -14.5$ cm on a movable sleigh allowing the toroidal source-detector distance D to range from 126 cm to 171 cm. The detector is a dedicated back-to-back Gridded Energy Analyzer (GEA), biased to filter out bulk electrons and ions [31] (see Fig. 1). After amplification, the back-side signal is subtracted from the front-side to reduce noise. Fast ions drift vertically due to the magnetic pitch-angle, gradient- and curvature-drifts. Turbulent electric fields affect the propagation of fast ions through localized $\mathbf{E}\times\mathbf{B}$-drifts [21, 32].

Previous experiments [32] and theoretical studies [21] using fluid tracer simulations with the Global Branginskii Solver [20, 27] have identified the non-diffusive regimes of the turbulent fast ion transport across magnetic field-lines. With fast ion injection energies of $E = 30$ eV or $E = 70$ eV, at an injection angle of $\approx 6°$ to the toroidal direction, the average fast ion Larmor radii amount to ≈ 5 mm and ≈ 8 mm respectively. Gyro- and drift-averaging over the turbulent electric fields are therefore stronger at $E = 70$ eV. After a brief ballistic transport phase, this leads to *subdiffusion* at all D considered here. For 30 eV ions, superdiffusion occurs instead, which smoothly transitions to quasi-diffusion around $D \gtrsim 100$ cm. At $D \geq 126$ cm, and we therefore associate $E = 30$ eV with a *super- to quasi-diffusive* regime. During initial studies in superdiffusion, transport appeared locally time intermittent as certain fast ion time-series showed significant skewness [11].

To generate such fast ion time-series, as shown in Fig. 2, the GEA signal is sampled for 1.5 s at a frequency of 250 kHz. Consistent with previous publications, the measured currents are divided by the circular detector area with $d = 8$ mm and thus presented as local fast ion current density time-series $J(t)$ at coordinates (R, Z). While the effective detector area may differ from this geometric estimate, this will only affect estimates for the total fast ion current I when used in Sec. IV, and compared to the conventions and fits in [22]. The ion-source undergoes on- and off-cycles at 23 Hz to distinguish the fast ion signal from residual noise.

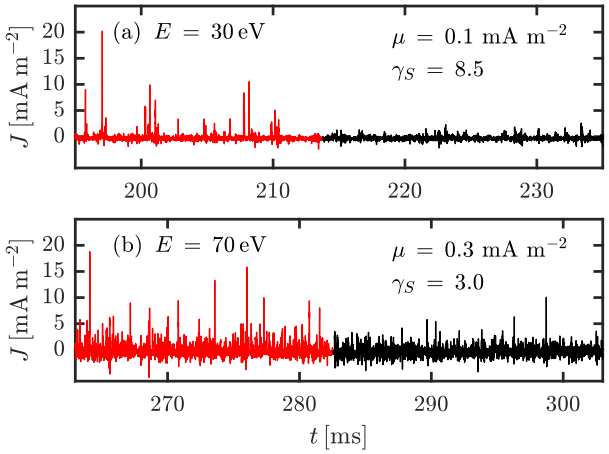

FIG. 2. Segments of the local time-series of fast ion current density $J(t)$ that feature the highest skewness at $D = 171$ cm and respective energy. The ion-source on-phases are indicated in red, off-phases in black. Distinct peaks are visible during the on-phase. The on-phase mean μ and skewness γ_S are given. For the mean, the off-phase value was subtracted. The locations (R, Z) of the GEA where these time-series were collected are marked in Fig. 3.

Time intermittency is quantified by each time-series' skewness (Fisher-Pearson coefficient [33]), as distinct, intermittent peaks in the signal strongly affect the higher order moments [2] (see Fig. 2).

III. RESULTS

We compute, for given D and E, poloidal mean and skewness profiles (see Fig. 3) to quantify intermittency. For the mean profiles, the time-average of $J(t)$ during the on-phases of the modulated ion-source is computed at

each poloidal location (R, Z) and the local off-phase average subtracted, to compensate acquisition offsets. The profile is then interpolated. The skewness-profiles are interpolated directly over the on-phase signal skewness $\gamma_{\mathcal{S}}$. For comparison, off-phase (noise) skewness never exceeds $\gamma_{\mathcal{N}} \approx 2$. We also investigated a noise-reduced skewness $\gamma_{\mathcal{J}}$ for statistically independent signal and noise

$$\gamma_{\mathcal{J}} = \frac{\sigma_{\mathcal{S}}^3 \gamma_{\mathcal{S}} - \sigma_{\mathcal{N}}^3 \gamma_{\mathcal{N}}}{(\sigma_{\mathcal{S}}^2 - \sigma_{\mathcal{N}}^2)^{3/2}} \tag{1}$$

, where $\sigma_{\mathcal{S}}$ denotes the standard deviation of the on-phase signal, and $\sigma_{\mathcal{N}}$ that of the off-phase signal. However this quantity quickly diverges in regions with low signal, so that $\gamma_{\mathcal{S}}$, the on-phase skewness, remains the measure for intermittency in what follows.

In practice, the total fast ion current I varies between profiles, depending on ion energy and source quality. This clearly affects the relative importance of contributions from the fast ions and noise to $\gamma_{\mathcal{S}}$ from one profile to the next. To allow a direct comparison between them, I is therefore estimated by numerically integrating the mean profile and all mean and skewness-profiles are then normalized to an averaged total current of $I_c = 2.85\,\mu$A (i.e. we "map" $\mapsto$),

$$J \mapsto cJ \quad , \quad \gamma_{\mathcal{S}} \mapsto \frac{c^3 \sigma_{\mathcal{S}}^3 \gamma_{\mathcal{S}} + (1-c^3)\sigma_{\mathcal{N}}^3 \gamma_{\mathcal{N}}}{(c^2 \sigma_{\mathcal{S}}^2 + (1-c^2)\sigma_{\mathcal{N}}^2)^{3/2}} \quad , \tag{2}$$

where we use the normalization factor $c = \frac{I_c}{I}$. Note that if we normalized with $I_c \gg I$ (i.e. towards an arbitrarily strong signal), one would find $\gamma_{\mathcal{S}} \mapsto \gamma_{\mathcal{J}}$ as expected.

As summarized in Fig. 4, the normalized skewness is above background (off-phase) level in many positions across all profiles. Lower energies show higher skewness, especially for longer D. Likewise, skewness increases further out in the LFS, provided the fast ions penetrate there measurably.

Especially for the 30 eV ions, the observed trends reflect the presence of distinct, intermittent peaks, which become increasingly rare toward the edges of the mean profile (see Fig. 2). As these peaks are most frequent near the maximum of the mean profile, they become less prominent compared to the local mean, which in turn limits the skewness there. These distinct peaks in fast ion current density consistently indicate that the fast ion beam at a given instant is more concentrated than its mean profile, especially for $E = 30\,$eV.

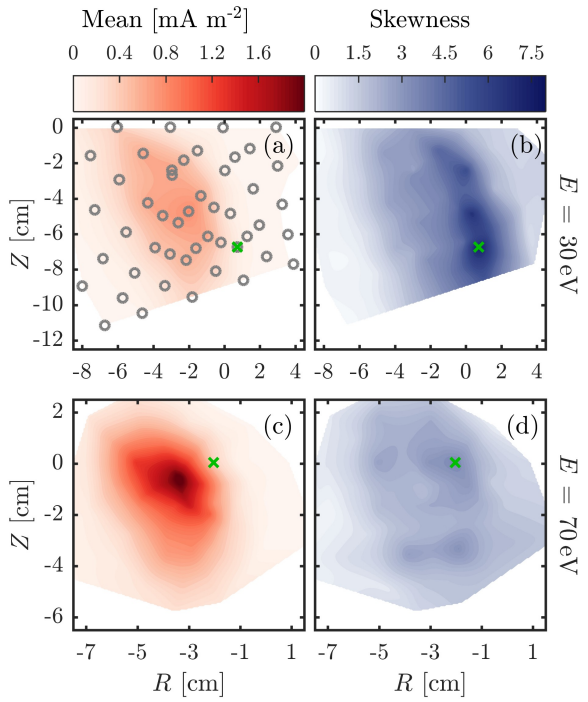

FIG. 3. Normalized mean and skewness-profiles at $D = 171\,$cm. Note the larger spread and reduced vertical drift at $E = 30\,$eV, as well as the lower peak current density and higher maximum skewness. The gray circles in a) indicate detector positions and green crosses the positions at which the time-series samples in Fig. 2 were acquired. The noise contributions from the background plasma increase significantly toward the interchange-mode on the HFS, and reduce the on-phase skewness here compared to the LFS.

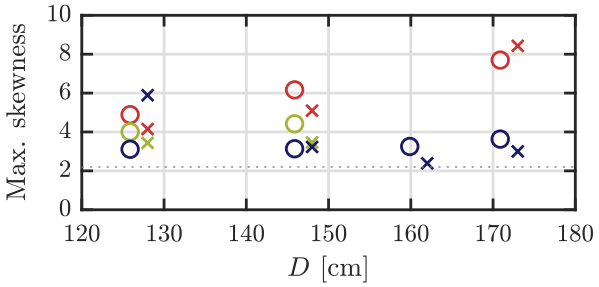

FIG. 4. Maximum normalized skewness for different source-detector distances D and fast ion energies E of 30, 50 and 70 eV in red, yellow and dark blue (circles, top to bottom) respectively. Crosses show values before normalization (see Eq. (2)) and are offset by $D = +2\,$cm for clarity. The dotted line indicates the maximum background value of $\gamma_{\mathcal{N}} = 2.2$.

IV. ANALYTICAL MODELING

Based on these characteristics of the fast ions, we have developed an analytical model for a setting in which a mean profile is built by the motion of a smaller, approximately rigid, instantaneous profile as detailed in Ref. [22], and outlined in Fig. 5. By describing the local mean profile $J(R, Z) = J(\mathbf{R})$ as the convolution of the instantaneous profile $j(\mathbf{R})$ and a displacement PDF $f(\mathbf{R})$, we describe the temporal average (first moment) $J = J_1$ of a time-series at $\mathbf{R}_0$ as the spatial average of $j(\mathbf{R} - \mathbf{R}_0)$ weighed by $f(\mathbf{R})$, which generalizes directly to arbitrary (non-central) moments of order q [22]

$$J_q(\mathbf{R}_0) = \iint j(\mathbf{R} - \mathbf{R}_0)^q \, f(\mathbf{R}) \, dR \, dZ \tag{3}$$

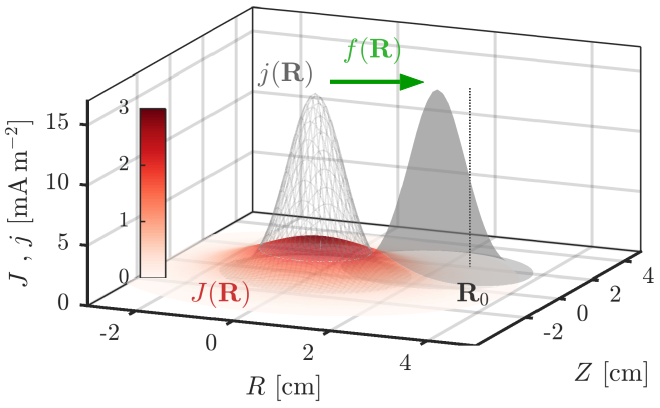

FIG. 5. Schematic of quantities in the analytical model, comprising the mean profile $J(\mathbf{R})$ and smaller instantaneous profile $j(\mathbf{R})$, which is deflected rigidly through the displacement PDF $f(\mathbf{R})$ towards a particular measurement position $\mathbf{R}_0$, where the detector area (aperture) is centered.

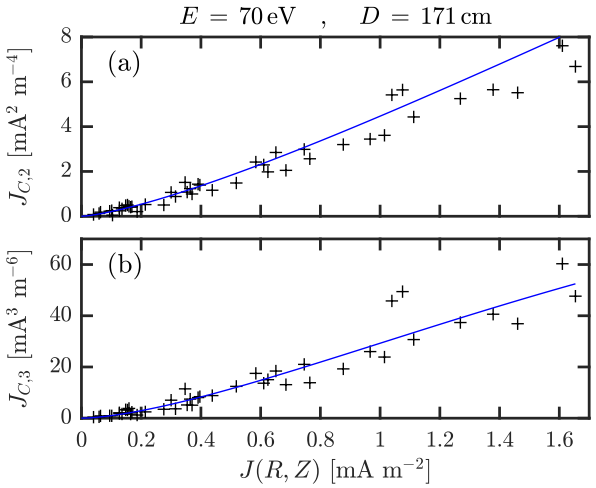

FIG. 6. Fit of the 2nd (a) and 3rd (b) central moment of the fast ion time-series at 70 eV and D = 171 cm, against the mean profile value $J(R,Z)$ as the only independent variable. The corresponding (normalized) profile is given in Fig.3(c).

A. Subdiffusion

As the simplest scenario, we firstly approximate both $j(\mathbf{R})$ and $f(\mathbf{R})$ (and therefore the mean profile $J(\mathbf{R})$) as symmetric 2D-Gaussians,

$$j(\mathbf{R}) = \frac{I}{2\pi\sigma_j^2}\, e^{-\frac{(R^2+Z^2)}{2\sigma_j^2}} = j_p\, e^{-\frac{(R^2+Z^2)}{2\sigma_j^2}} \quad (4)$$

$$f(\mathbf{R}) = \frac{1}{2\pi\sigma_f^2}\, e^{-\frac{(R^2+Z^2)}{2\sigma_f^2}} \quad (5)$$

$$\Rightarrow J(\mathbf{R}) = \frac{I}{2\pi\sigma_J^2}\, e^{-\frac{(R^2+Z^2)}{2\sigma_J^2}} \quad , \quad (6)$$

where σ denotes the respective standard deviations in both the radial and vertical direction and we have $\sigma_J^2 = \sigma_j^2 + \sigma_f^2$. Assuming a total detectable current I, the parameter $j_p = \frac{I}{2\pi\sigma_j^2}$ denotes the peak of the instantaneous current density profile $j(\mathbf{R})$, and hence the maximum in any time-series of the profile, pending noise. For such Gaussian profiles, one can obtain a concise analytical expression for the moments J_q

$$J_q(R,Z) = q^{-1} s_q \rho^{(2-2s_q)} j_p^{(q-s_q)} J(R,Z)^{s_q} \quad (7)$$
$$\text{with} \quad s_q = \left[1-\rho^2\left(1-q^{-1}\right)\right]^{-1} \quad ,$$

where the parameter $\rho = \frac{\sigma_j}{\sigma_J}$ denotes the ratio of width of the instantaneous time-average profile. Using Eq. (7), the skewness of any prospective local time-series can be predicted solely from the measurement of the mean profile, once the parameters ρ and j_p parameters are set. While they may be given from prior knowledge of the system or extracted from simulations (see [22], Sec.V), we leave them as free parameters for least-square fitting moments predicted from the model to those of the measured time-series. Specifically, to assess the validity of this Gaussian model for each subdiffusive profile, we perform simultaneous least-square fits with the second and third *central* moments $J_{C,[2,3]}$

$$\sigma_{\mathcal{S}}^2 - \sigma_{\mathcal{N}}^2 \approx J_{C,2} = J_2 - J^2 \quad (8)$$
$$\gamma_{\mathcal{S}}\sigma_{\mathcal{S}}^3 - \gamma_{\mathcal{N}}\sigma_{\mathcal{N}}^3 \approx J_{C,3} = J_3 - 3JJ_2 + 2J^3 \quad . \quad (9)$$

Again, the skewness (γ) and standard deviation (σ) from the ion-source on-phase signals are indicated with $\mathcal{S}$. The second term on the LHS removes noise contributions ($\mathcal{N}$), measured during off-phases. We consider all (R,Z) with $J(R,Z) > 0.04\,\text{mAm}^{-2}$, being twice the typical measurement uncertainty from bootstrap error calculations. Since I enters in a fit parameter, no normalization to common total currents is undertaken. One such fit result for $J_{C,[2,3]}$, shown in Fig. 6, demonstrates the potential effectiveness of the method. Again, it should be noted, that the only variable is $J(R,Z)$ itself. To succinctly asses the predictive quality for the skewness (see Fig. 7) we solve for $\gamma_{\mathcal{S}}$ in Eq. (9)

$$\gamma_{\mathcal{S}} \approx \frac{J_{C,3} + \gamma_{\mathcal{N}}\sigma_{\mathcal{N}}^{3/2}}{\left(J_{C,2}+\sigma_{\mathcal{N}}^2\right)^{3/2}} \quad . \quad (10)$$

There is good agreement with measurements, typically within 20%. Larger over- or under-estimates (see Fig. 7(a)) may be partly due to temporary fluctuations in the injected fast ion current, that were avoided in more stable settings with lower currents (see Fig. 7(b-c)). Comparing with a raw time-series in Fig. 2(b), the corresponding $j_p \approx 15\,\text{mAm}^{-2}$ agrees well with the most distinct peaks. Taking I again from integrations, we hence deduce an instantaneous beam width of $\sigma_n \approx 5\,\text{mm}$, which is consistent with results from numerical investigations [22]. With a fitted $\rho \geq 0.75$, we find however that this model provides an underestimated width of the mean profiles

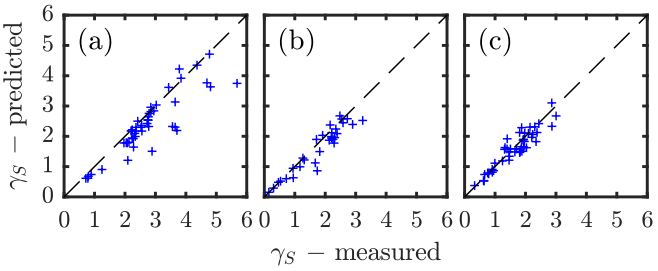

FIG. 7. On-phase skewness γ_S at $D = \{126, 146, 171\}$ cm (a,b,c) for 70 eV profiles as predicted from Eq. (10) vs. measured values. The estimated total fast ion currents are $I = \{5.04, 2.97, 2.36\}\mu$A.

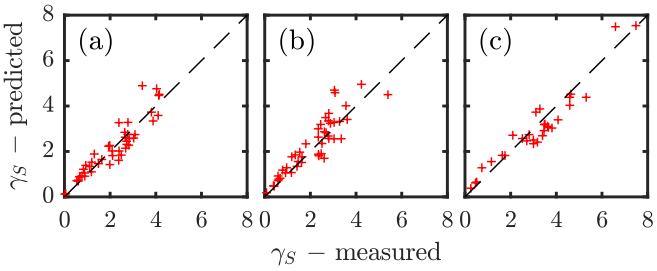

FIG. 8. On-phase skewness γ_S at $D = \{126, 146, 171\}$ cm (a,b,c) for 30 eV profiles as predicted from Eq. (10) (with $J_{C[2,3]}$ from Eq. (12,13)) vs. measured values. The estimated total fast ion currents are $I = \{2.35, 2.5, 3.2\}\,\mu$A.

by up to a factor of 2. This shows that the features of subdiffusive profiles cannot be entirely reflected by the Gaussian model, despite the accuracy in the fits for moments and skewness. This discrepancy is exacerbated in the larger super- to quasi-diffusive profiles, especially since the highest skewness is found in their heavy tails.

B. Super- to quasi-diffusion

However, we can reasonably assume a small width of $j(\mathbf{R})$, i.e. $\rho \ll 1$ in this case. This allows us to expand $f(\mathbf{R})$ directly in Eq. (3) as a series about $\mathbf{R}_0$ and find $f(\mathbf{R}) \approx J(\mathbf{R})$ to approximately 2nd order in ρ without any assumptions on the form of $f(\mathbf{R})$. In this limit, one therefore has

$$J_q(R,Z) \approx J(R,Z) \iint n(\mathbf{R})^q \, dR\, dZ + \mathcal{O}\left(\frac{\sigma_n^2}{2}\left(\frac{\partial^2 J}{\partial R^2} + \frac{\partial^2 J}{\partial Z^2}\right)\right) \tag{11}$$

and can therefore also find simple analytical expressions for the central moments $J_{C,[2,3]}$ (cf [22], Sec.IV),

$$J_{C,2} = \frac{1}{2} j_p J - J^2 \tag{12}$$

$$J_{C,3} = \frac{1}{3} j_p^2 J - \frac{3}{2} j_p J^2 + 2J^3 \tag{13}$$

as well as γ_S again according to Eq. (10). The remaining parameter j_p is left again free to perform a simultaneous least-square fit of predicted $J_{C,[2,3]}$ on the time-resolved data. Fig. 8 shows the resulting γ_S in each super- to quasi-diffusive profile.

Again, predictions agree well with measurements, pending noise and fluctuations in the injected current. The fitted j_p follow the trend of total current I across the different profiles and the value of e.g. $j_p \approx 14\,\mathrm{mAm}^{-2}$ for $D = 171$ cm corresponds well to the most distinct peaks in the time-series of Fig. 2(a) . In the 70 eV case, the condition $\rho \ll 1$ stops being valid and thus the Gaussian approximations remain favorable.

V. CONCLUSION

In summary, we have shown experimentally that time intermittency is not exclusive to any particular non-diffusive transport regime for fast ions in TORPEX turbulent plasmas. In this case it arises from the motion of a concentrated instantaneous fast ion profile resulting in a larger mean profile. With larger mean profiles towards quasi- and superdiffusion, as well as longer fast ion propagation times, the prevalence of intermittency increases, as instantaneous peaks can become more prominent with respect to the local mean. The ubiquity of intermittency is accurately predicted by an analytical fast ion beam model, which may be of direct interest in similar settings, e.g. in beam physics, and illustrates the general importance of identifying the system specific sources of time intermittent behavior when analyzing non-diffusive transport. Although the specific systems are quite different from our setting, the apparent reduction of the impact of intermittency in situations with increased orbit-averaging (our 70 eV case) could be of interest in other domains in plasma physics, e.g. turbulent fast ion losses in fusion devices [34, 35] or the propagation of Solar Energetic Particles [12], as e.g. for models of SEP dropouts, which feature meandering magnetic flux ropes along which SEPs propagate [36].

ACKNOWLEDGMENTS

We gratefully acknowledge the support of the mechanical, electrical and electronic workshops at the Swiss Plasma Center

This work has been carried out within the framework of the EUROfusion Consortium and has received funding from the Euratom research and training programme 2014 - 2018 and 2019 - 2020 under grant agreement No 633053. The views and opinions expressed herein do not necessarily reflect those of the European Commission.

This work was partly funded by the Swiss National Science Foundation.

[1] A. F. Hussain, Journal of Fluid Mechanics **173**, 303 (1986).
[2] Z.-S. She, E. Jackson, and S. A. Orszag, Nature **344**, 226 (1990).
[3] R. Metzler and J. Klafter, Phys. Rep. **339**, 1 (2000).
[4] E. W. Montroll and G. H. Weiss, J. Math. Phys. **6**, 167 (1965).
[5] R. Metzler and J. Klafter, Physical Review E **61**, 6308 (2000).
[6] F. Alouani-Bibi and J. A. Le Roux, Astrophys. J. **781**, 93 (2014).
[7] D. El Masri, L. Berthier, and L. Cipelletti, Phys. Rev. E **82**, 031503 (2010).
[8] R. L. Martin, D. J. Jerolmack, and R. Schumer, J. Geophys. Res. - Earth **117** (2012).
[9] P. Paradisi, R. Cesari, A. Donateo, D. Contini, and P. Allegrini, Nonlinear Proc. Geoph. **19**, 113 (2012).
[10] V. Budaev, S. Takamura, N. Ohno, and S. Masuzaki, Nucl. Fusion **46**, S181 (2006).
[11] A. Bovet, A. Fasoli, and I. Furno, Phys. Rev. Lett. **113**, 225001 (2014).
[12] G. Zimbardo, E. Amato, A. Bovet, F. Effenberger, A. Fasoli, H. Fichtner, I. Furno, K. Gustafson, P. Ricci, and S. Perri, J. Plasma Phys. **81** (2015).
[13] Y. Pomeau and P. Manneville, Commun. Math. Phys. **74**, 189 (1980).
[14] G. Zumofen and J. Klafter, Physical Review E **47**, 851 (1993).
[15] R. Artuso and R. Burioni, in *Large Deviations in Physics* (Springer, 2014) pp. 263–293.
[16] L. Seuront and H. E. Stanley, P. Natl. Acad. Sci.- Biol. **111**, 2206 (2014).
[17] S. H. Müller, A. Diallo, A. Fasoli, I. Furno, B. Labit, and M. Podestà, Phys. Plasmas **14**, 110704 (2007).
[18] A. Fasoli, A. Burckel, L. Federspiel, I. Furno, K. Gustafson, D. Iraji, B. Labit, J. Loizu, G. Plyushchev, P. Ricci, C. Theiler, A. Diallo, S. H. Müller, M. Podestà, and F. Poli, Plasma Phys. Contr. F. **52**, 124020 (2010).
[19] I. Furno, F. Avino, A. Bovet, A. Diallo, A. Fasoli, K. Gustafson, D. Iraji, B. Labit, J. Loizu, S. Müller, *et al.*, J. Plasma Phys. **81** (2015).
[20] P. Ricci, F. D. Halpern, S. Jolliet, J. Loizu, A. Mosetto, A. Fasoli, I. Furno, and C. Theiler, Plasma Phys. Contr. F. **54**, 13. 124047 (2012).
[21] K. Gustafson, P. Ricci, A. Bovet, I. Furno, and A. Fasoli, Phys. Plasmas **19**, 062306 (2012).
[22] M. Baquero-Ruiz, F. Manke, I. Furno, A. Fasoli, and P. Ricci, Phys. Rev. E **98**, 032111 (2018).
[23] M. Baquero-Ruiz, F. Avino, O. Chellai, A. Fasoli, I. Furno, R. Jacquier, F. Manke, and S. Patrick, Rev. Sci. Instrum. **87**, 113504 (2016).
[24] M. Podestà, A. Fasoli, B. Labit, M. McGrath, S. Müller, and F. Poli, Plasma Phys. Contr. F. **48**, 1053 (2006).
[25] F. M. Poli, M. Podestà, and A. Fasoli, Phys. Plasmas **14**, 052311 (2007).
[26] B. Labit, I. Furno, A. Fasoli, A. Diallo, S. H. Müller, G. Plyushchev, M. Podestà, and F. M. Poli, Phys. Rev. Lett. **98**, 255002 (2007).
[27] P. Ricci, C. Theiler, A. Fasoli, I. Furno, B. Labit, S. Müller, M. Podestà, and F. M. Poli, Phys. Plasmas **16**, 055703 (2009).
[28] I. Furno, B. Labit, M. Podestà, A. Fasoli, S. H. Müller, F. M. Poli, P. Ricci, C. Theiler, S. Brunner, A. Diallo, and J. Graves, Phys. Rev. Lett. **100** (2008).
[29] S. H. Müller, C. Theiler, A. Fasoli, I. Furno, B. Labit, G. R. Tynan, M. Xu, Z. Yan, and J. H. Yu, Plasma Phys. Contr. F. **51**, 055020 (2009).
[30] C. Theiler, I. Furno, P. Ricci, A. Fasoli, B. Labit, S. H. Müller, and G. Plyushchev, Phys. Rev. Lett. **103**, 065001 (2009).
[31] G. Plyushchev, A. Diallo, A. Fasoli, I. Furno, B. Labit, S. H. Müller, M. Podestà, F. M. Poli, H. Boehmer, W. W. Heidbrink, and Y. Zhang, Rev. Sci. Instrum **77**, 10F503 (2006).
[32] A. Bovet, A. Fasoli, P. Ricci, I. Furno, and K. Gustafson, Phys. Rev. E **91**, 041101 (2015).
[33] R. Shanmugam and R. Chattamvelli, *Statistics for scientists and engineers* (Wiley Online, 2015).
[34] W. Heidbrink and G. Sadler, Nucl. Fusion **34**, 535 (1994).
[35] A. Fasoli, C. Gormenzano, H. Berk, B. Breizman, S. Briguglio, D. Darrow, N. Gorelenkov, W. Heidbrink, A. Jaun, S. Konovalov, *et al.*, Nuclear Fusion **47**, S264 (2007).
[36] T. Laitinen, A. Kopp, F. Effenberger, S. Dalla, and M. Marsh, Astron. Astrophys. **591**, A18 (2016).